Journal of Alloys and Compounds 507 (2010) 105–111

Contents lists available at ScienceDirect

Journal of Alloys and Compounds

journal homepage: www.elsevier.com/locate/jallcom

Synthesis of rare earth (Pr, Nd, Sm, Eu and Gd) hydroxide and oxide nanorods (nanobundles) by a widely applicable precipitation route

Ying Xin[a], Zhongpeng Wang[a], Yongxin Qi[b], Zhaoliang Zhang[a,*], Shuxiang Zhang[a]

[a] Shandong Provincial Key Laboratory of Fluorine Chemistry and Chemical Materials, College of Chemistry and Chemical Engineering, University of Jinan, 106 Jiwei Rd., Jinan 250022, China
[b] School of Material Science and Technology, Shandong University, Jinan 250100, China

ARTICLE INFO

Article history:
Received 19 June 2010
Received in revised form 13 July 2010
Accepted 14 July 2010
Available online 24 July 2010

Keywords:
Rare earth alloys and compounds
Nanostructured materials
Precipitation
Anisotropy

ABSTRACT

Rare earth hydroxide and oxide nanorods (nanobundles) have been synthesized without the addition of any templates/surfactants by a simple precipitation method under ambient temperature and pressure. The products are characterized by X-ray diffraction (XRD), transmission electron microscopy (TEM), field-emission scanning electron microscopy (FESEM), thermogravimetry (TG) and N_2 adsorption/desorption. It is demonstrated that the rare earth hydroxide nanorods (nanobundles) have the diameter of 10–150 nm and the length of 30–600 nm. The corresponding oxides can be obtained by calcination, which preserved the nanorod (nanobundle) morphologies though a small shrinkage in sizes is observed. The influences of the aging time and precipitation agent on the formation of nanorods (nanobundles) are investigated. Accordingly the crystallization mechanism is proposed. The nucleation and growth of the hydroxide nanorods may occur in the precipitation process at relatively low (room) temperature and normal pressure without a long-time and high-temperature (pressure) hydrothermal treatment. The photoluminescence (PL) analysis is used to investigate the optical properties of the Eu_2O_3 nanobundles and a broadened luminescent spectrum is observed. The precipitation method is simple, highly reproducible, inexpensive, and widely applicable for the large-scale industrial production.

1. Introduction

Rare earth compounds possess wide applications in high-performance luminescent devices [1–3], magnets [4], catalysts [5–7], and other functional materials [8] because of their unique physical and chemical properties originating from the 4f shell of electrons. Most of these properties are highly sensitive to the composition and structure, especially to the complexation state and the crystal field of the matrix in which rare earth ions are trapped [9,10]. Therefore, rare earth nanostructures are provided with superior properties compared with bulk materials. Among the various nanostructures, 1D nanostructures with their inherent anisotropy have attracted much interests due to their enhanced properties and promising applications [11,12], including nanowires [13,14], nanotubes [15,16], nanobelts [17], and especially nanorods [18–20]. For example, the Eu_2O_3 nanorods generate a red emission band, which may be applied in optoelectronic devices [21,22]. The Sm_2O_3 nanorods have high hydrocarbon selectivity for the CO hydrogenation [23]. The Pr_6O_{11} nanorods supported with Au exhibit superior catalytic activity for CO oxidation [24].

Accordingly, considerable efforts have been spent on the synthesis of rare earth hydroxide (oxide) nanorods. The solvothermal/hydrothermal treatment in the presence or absence of templates/surfactants at higher temperature is the most used strategy. Wang and Li obtained a series of rare earth hydroxide nanowires through the preparation of colloidal lanthanide hydroxide at room temperature, with subsequent hydrothermal treatment at 180 °C for about 12 h [25]. Zhang et al. successfully synthesized $La(OH)_3$, $Nd(OH)_3$, $Sm(OH)_3$, $Gd(OH)_3$ and $Dy(OH)_3$ nanorods via hydrothermal method, but triethylamine was added as both alkaline agent and complexing agent [26]. The microwave [27,28], ultrasound [29] and sol–gel [23] methods have also been developed. Although these methods provide effective routes to fabricate 1D nanorods, special apparatus (using autoclave), complicated process (to remove templates/surfactants), and/or rigid conditions (high-temperature and pressure) are needed, which are severely adverse to the large-scale production. Therefore, it is still very significant to develop a simple and efficient approach without these drawbacks. Yan et al. got the $Pr(OH)_3$ nanorods by a template-free precipitation process at 100 °C [30]. Wu et al. found a similar method for $Eu(OH)_3$ [31]. Recently, Qian et al. reported a simple

* Corresponding author. Tel.: +86 531 89736032; fax: +86 531 89736032.
E-mail addresses: zhangzhaoliang@sdu.edu.cn, chm_zhangzl@ujn.edu.cn (Z. Zhang).

0925-8388/$ – see front matter © 2010 Elsevier B.V. All rights reserved.
doi:10.1016/j.jallcom.2010.07.109

Table 1
Textural property of $RE(OH)_3$ and REO_x.

RE	$RE(OH)_3$ lattice constants (Å)		$RE(OH)_3$ (nm)		REO_x lattice constants (Å)	REO_x (nm)		BET surface area (m^2/g)	
	a	*c*	Diameter	Length	*a*	Diameter	Length	$RE(OH)_3$	REO_x
Pr	6.456	3.769	10–30	30–100	5.467	10–20	30–90	62.9	43.9
Nd	6.418	3.743	20–30	70–150	11.072	10–25	50–120	65.7	50.8
Sm	6.368	3.683	30–150	150–350	10.915	20–50	100–250	42.3	29.4
Eu	6.352	3.653	50–150	200–600	10.863	50–100	150–500	36.2	26.1
Gd	6.329	3.631	50–150	150–600	10.818	50–100	150–600	62.5	22.6

solution route for the synthesis of light rare earth (La, Pr, Nd, Sm, Eu and Gd) hydroxide nanorods [32]. The mixed solution of rare earth oxides and hydrochloric acid were rapidly adjusted to the pH value of 13 using 5 M NaOH solution, which was then aged for 30 days. The method is a great inspiration to us because any surfactants or templates were used.

The conventional precipitation is simple, easy and environmentally benign, thus it is much more suitable for industrial production compared with the sol–gel and hydrothermal methods [33]. Herein, we reported the synthesis of rare earth (denoted as RE: Pr, Nd, Sm, Eu and Gd) hydroxide nanorods (nanobundles) through a facile precipitation route which is free of any templates/surfactants at room temperature and pressure. The as-prepared hydroxide nanorods (nanobundles) can be transformed into the corresponding rare earth oxides, which preserved the nanorod (nanobundle) morphology. The significant finding is that the rare earth hydroxides without the aging process show the well crystalline nanorod morphology, suggesting that the nucleation and growth of nanorods took place in precipitation process.

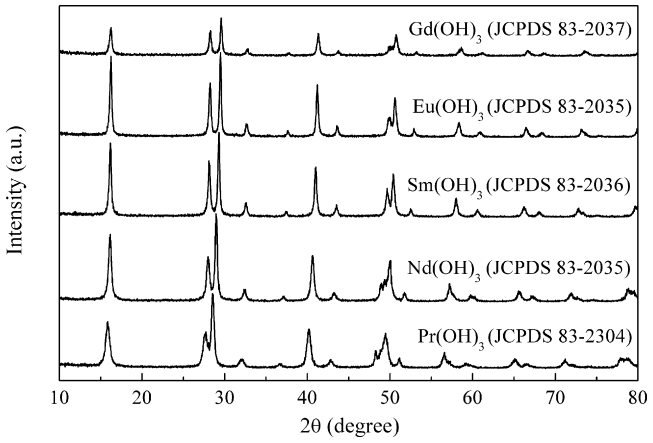

Fig. 1. XRD patterns of $RE(OH)_3$ synthesized using ammonia as the precipitate agent aging for 96 h and after drying (before calcination). The JCPDS numbers were also given.

2. Experimental methods

2.1. Synthesis method

All of the chemicals used in this experiment were of analytical grade and used without further purification. Rare earth hydroxides ($RE(OH)_3$) were prepared by a simple precipitation method at room temperature and pressure. In a typical procedure, the water solution (100 ml) containing 0.018 mol $RE(NO_3)_3{\cdot}6H_2O$ was introduced dropwise into 150 ml $NH_3{\cdot}H_2O$ solution (25 wt.%) under vigorous stirring. The resultant suspension was maintained in a sealed glass beaker and aged at room temperature for different time (0, 48, 96 h). After filtration, the precipitate was washed several times with deionized water, and dried at 100 °C in air overnight. Rare earth oxides (REO_x) were obtained by calcination of the correspond-

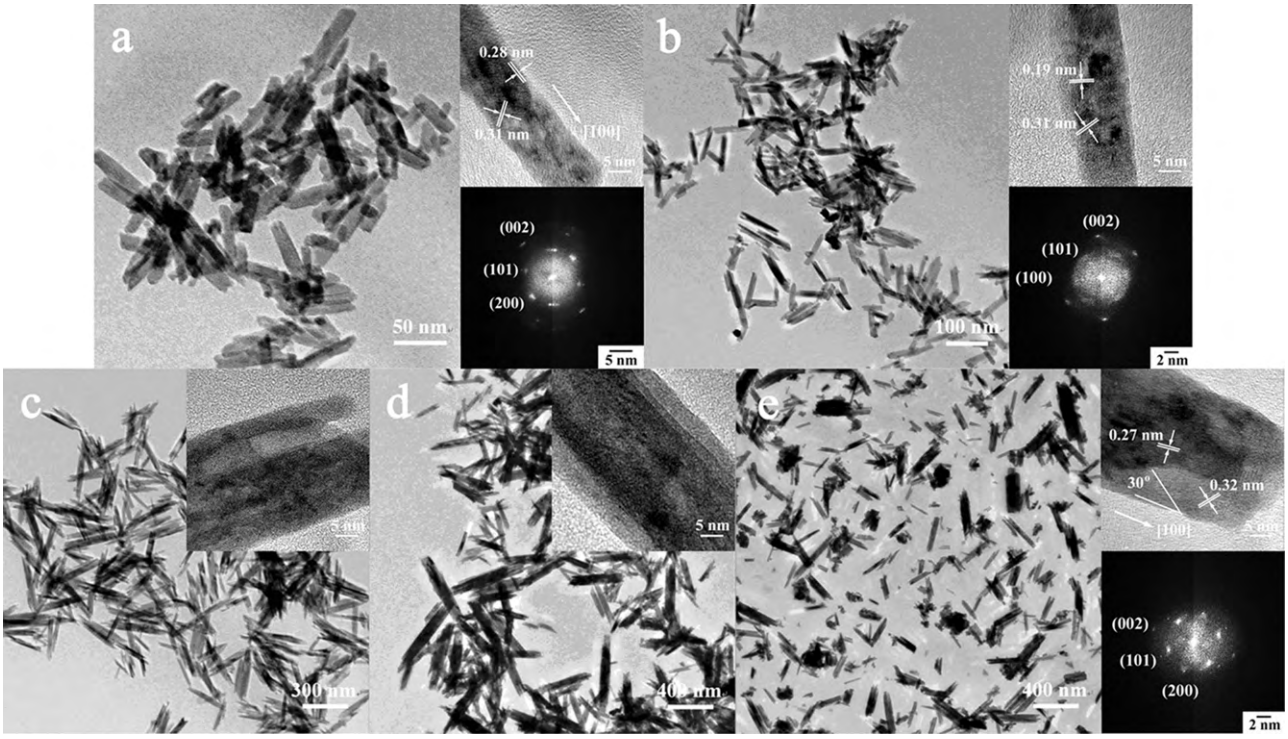

Fig. 2. TEM images of $RE(OH)_3$ synthesized using ammonia as the precipitate agent aging for 96 h and after drying (before calcination): (a) $Pr(OH)_3$; (b) $Nd(OH)_3$; (c) $Sm(OH)_3$; (d) $Eu(OH)_3$; (e) $Gd(OH)_3$. The insets are the HRTEM images and the corresponding FFT patterns.

ing $RE(OH)_3$ at 650 °C for 2 h in air. For reference, the bulk Eu_2O_3 was prepared by thermal decomposition of europium nitrate at 650 °C for 2 h in air.

2.2. Characterization methods

X-ray powder diffraction (XRD) patterns were recorded on a Rigaku D/max-rc diffractmeter employing Cu $K_(\alpha)$ radiation. The unit cell parameters were obtained by refining the peak positions of the XRD patterns with a least square method using the equations of $1/d^2 = 4(h^2 + hk + k^2)/3a^2 + l^2/c^2$ and $1/d^2 = (h^2 + k^2 + l^2)/a^2$ for hexagonal (a and c) and cubic (c) structure, respectively.

High-resolution transmission electron microscopy (HRTEM) was conducted on a JEOL JEM-2010 at an accelerating voltage of 200 kV. Field-emission scanning electron microscopy (FESEM) images were obtained with a JEOL SU70 microscope.

Thermogravimetry (TG) of the rare earth hydroxides was carried out using a PerkinElmer Diamond TG/DTA with a heating rate of 10 °C/min in a flowing air atmosphere from room temperature to 800 °C.

The Brunauer–Emmett–Teller (BET) surface area and pore structure were measured by N_2 adsorption/desorption by means of a Micromeritics 2020 M instrument.

The photoluminescence (PL) spectra were taken on a HITACHI F-4600 fluorescence spectrophotometer with a 150 W Xenon lamp as an excitation source.

3. Results and discussion

Fig. 1 shows the XRD patterns of the $RE(OH)_3$ samples. All diffraction peaks were indexed to the hexagonal phase. The lattice constants (a and c) were calculated and listed in Table 1. The shift to higher angles for the diffraction peaks and the corresponding decrease in lattice constants from Pr to Gd hydroxides can be attributed to the well-known lanthanide contraction [34]. Fig. 2 shows the TEM (HRTEM) images of the $RE(OH)_3$ samples. Evidently, the individual nanorods are observed for $Pr(OH)_3$ and $Nd(OH)_3$, while the bundles of nanorods appeared for $Sm(OH)_3$, $Eu(OH)_3$ and $Gd(OH)_3$. As shown in Table 1, the nanobundles are much thick and long. Based on the HRTEM images and the corresponding FFT patterns, the nanorod itself is a single crystal, while the nanobundles might be polycrystalline. Although all nanorods are randomly dispersed, the growth direction is along c-axis. Take the $Gd(OH)_3$ nanorod as an example, the interplanar spacing of 0.32 nm and 0.27 nm is consistent with the d spacing value of (1 1 0) and (2 0 0) planes, respectively. The growth direction of the nanorod makes an angle of about 30° with (1 1 0) lattice planes and is parallel to the (2 0 0) lattice plane, which means that it is along [1 0 0] direction [29,35].

Aging is an important process for the anisotropic growth of nanorods [36]. With a view to investigate the morphological evolution of the products, the time-dependent experiments are performed by collecting small portions of the reacting products from time to time for both XRD and TEM analysis. Take $Nd(OH)_3$ as an example, as shown in Fig. 3a, the $Nd(OH)_3$ precipitate with hexagonal structure can be obtained without the aging process (0 h). The weak and wide diffraction peaks indicate the small size

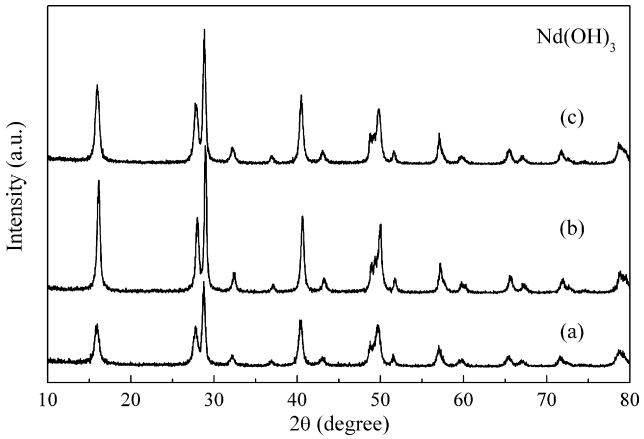

Fig. 3. XRD patterns of $Nd(OH)_3$ synthesized using ammonia as the precipitation agent aging for (a) 0 h, (b) 48 h, and (c) 96 h and after drying (before calcination).

or the poor crystalline nature of the obtained nanocrystals. On extending the aging time, the diffraction peaks become sharper and stronger, implying that the crystallinity of the products is high (Fig. 3b and c). The corresponding TEM images are presented in Fig. 4. The irregular short nanorods of $Nd(OH)_3$ are directly obtained at such a low temperature after the precipitation reaction without aging. This result is distinct from the previous reports which proposed that the nucleation and crystal growth of nanorods should be accomplished after a long-time and high-temperature hydrothermal treatment [10,21,25,32,37]. We speculate that a fraction of

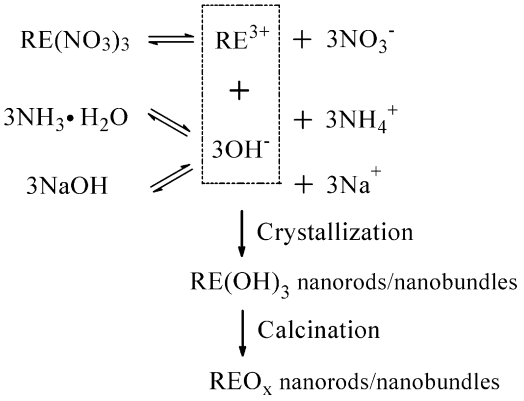

Scheme 1. The possible formation mechanism of the $RE(OH)_3$ and REO_x nanorods (nanobundles).

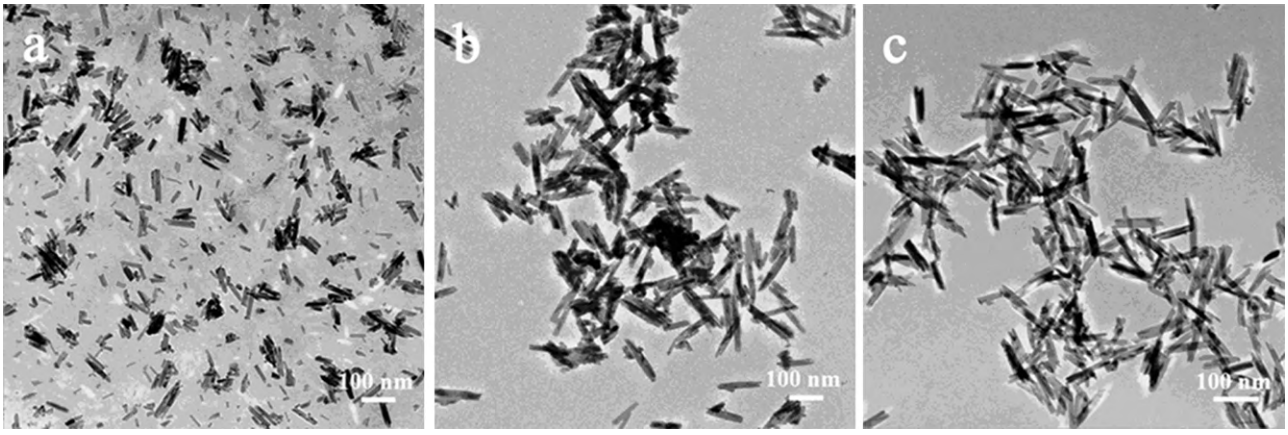

Fig. 4. TEM images of $Nd(OH)_3$ synthesized using ammonia as the precipitation agent aging for (a) 0 h, (b) 48 h, and (c) 96 h and after drying (before calcination).

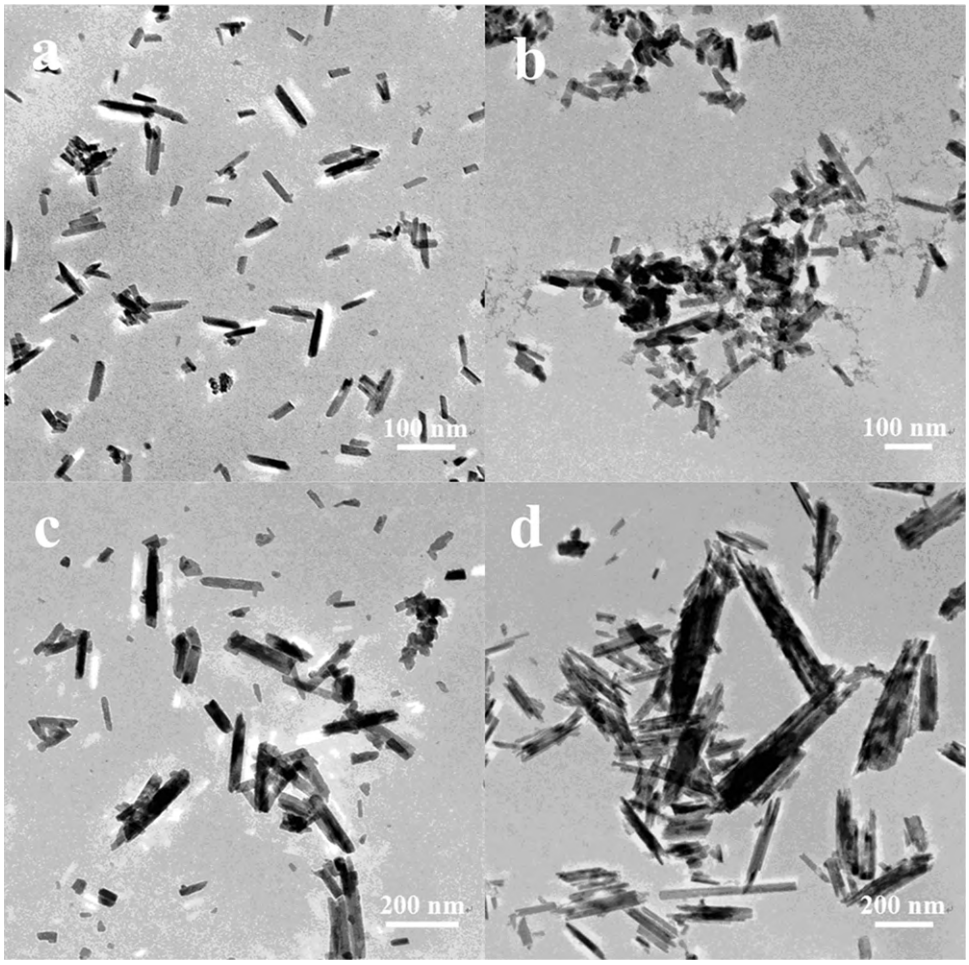

Fig. 5. TEM images of (a) $Pr(OH)_3$, (b) $Sm(OH)_3$, (c) $Eu(OH)_3$, (d) $Gd(OH)_3$ synthesized using ammonia as the precipitation agent aging for 0 h and after drying (before calcination).

$Nd(OH)_3$ nuclei can rapidly form and grow into a certain extent in precipitation process at room temperature. As shown in Fig. 5, the similar results were observed for other rare earth hydroxide nanorods (nanobundles).

The effects of the precipitation agents are also studied during the preparation of the $Eu(OH)_3$ sample. When ammonia is substituted by NaOH (2 M), the $Eu(OH)_3$ precipitation is also obtained under the same experimental conditions. As shown in the TEM image in Fig. 6b, the nanorods can be found with higher aspect ratio and more uniform morphologies compared with the counterpart (shown in Fig. 6a), suggesting that NaOH, which is stronger in basicity than ammonia, can accelerate the nucle-

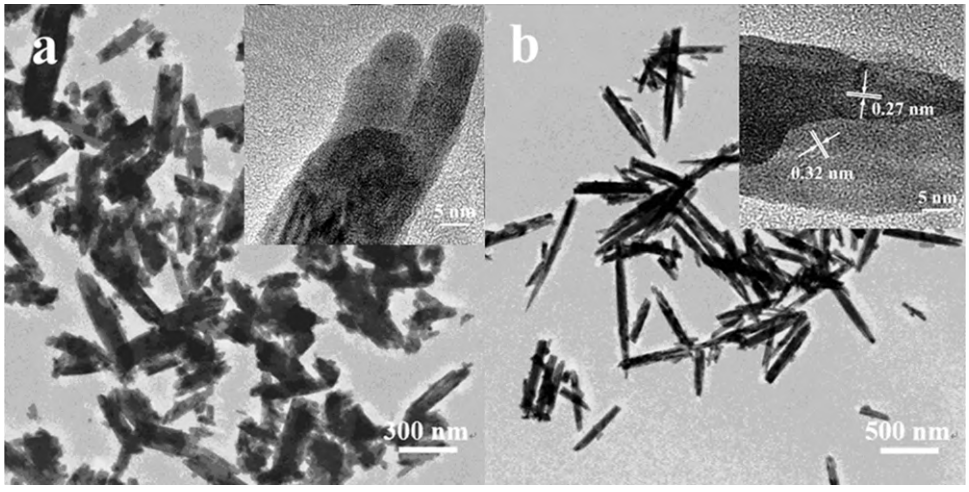

Fig. 6. TEM images of $Eu(OH)_3$ synthesized using (a) ammonia, (b) NaOH as the precipitation agent aging for 48 h and after drying (before calcination). The insets are the HRTEM images.

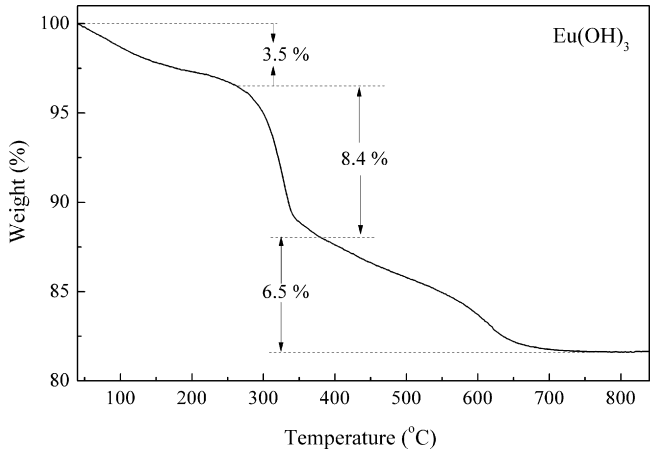

Fig. 7. TG pattern of $Eu(OH)_3$ synthesized using ammonia as the precipitation agent aging for 96 h and after drying (before calcination).

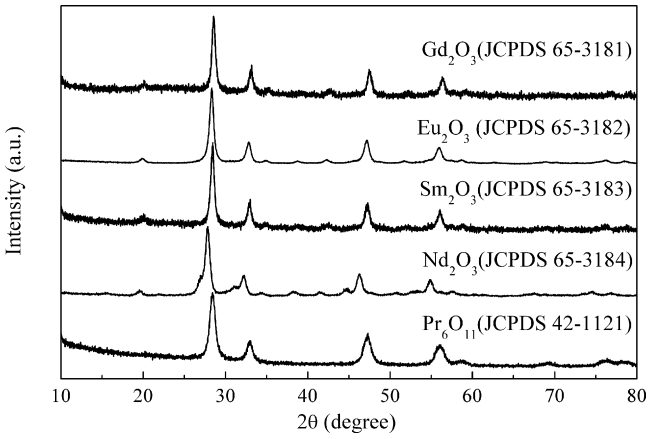

Fig. 8. XRD patterns of REO_x obtained by calcination of $RE(OH)_3$ at 650 °C for 2 h in air. The JCPDS numbers were also given.

ation and crystal growth. The above experiments confirm that the morphologies of the $RE(OH)_3$ nanorods (nanobundles) can be controlled through adjusting the aging time and precipitation agent.

It is well-known that the crystal growth and morphology are controlled by the extrinsic and intrinsic factors in the reaction solution, such as the diffusion of reaction species, crystal structure, surface energy and chemical potential [38,39]. In the synthetic

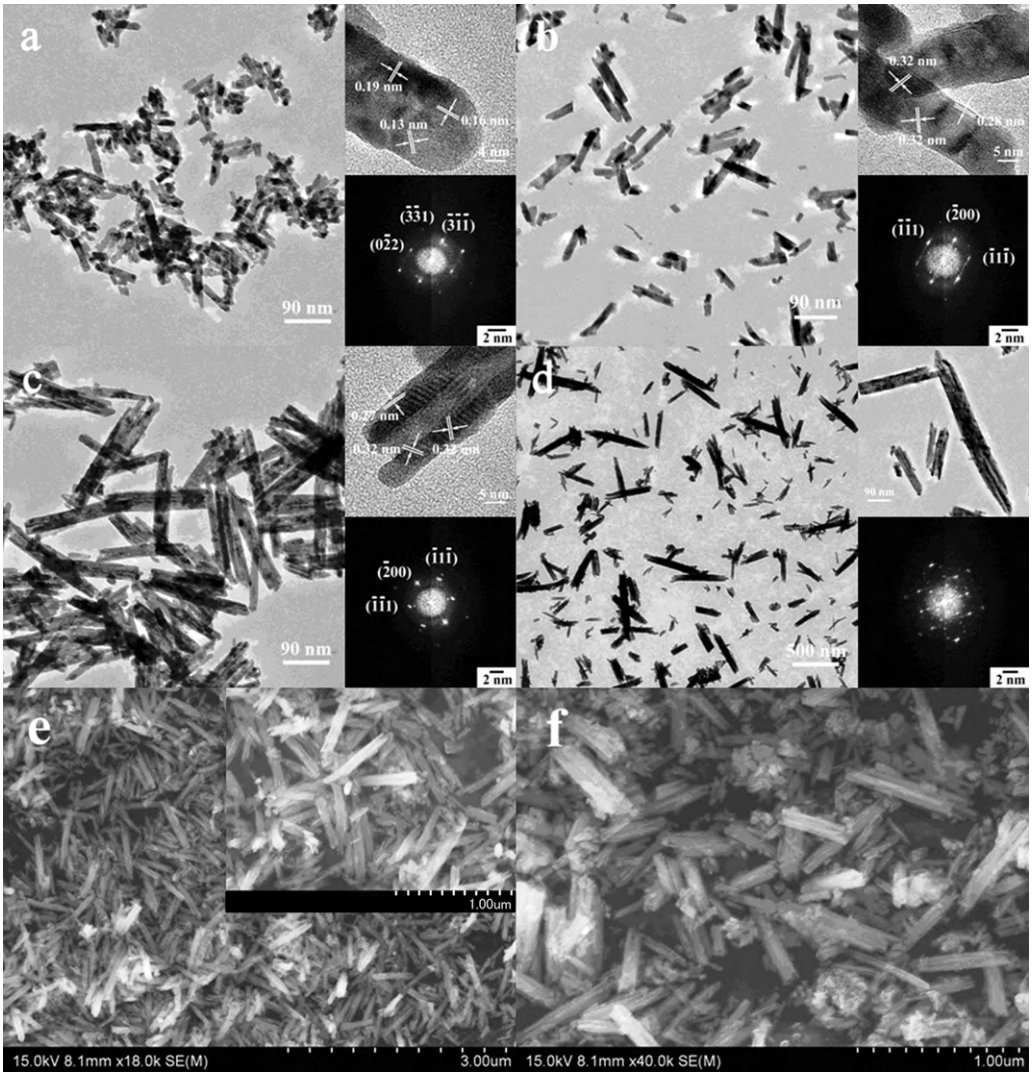

Fig. 9. The morphologies of REO_x obtained by calcination of $RE(OH)_3$ at 650 °C for 2 h in air. TEM images of (a) Pr_6O_{11}, (b) Nd_2O_3, (c) Sm_2O_3, and (d) Eu_2O_3. The insets are the HRTEM (high magnification) images and the corresponding FFT patterns. FESEM images of (e) Eu_2O_3, and (f) Gd_2O_3.

process of the present study, there is no template or surfactant to guide the directional growth of nanorods. Thus, it is reasonable to imagine that the driving force for the anisotropic growth of the $RE(OH)_3$ nanorods derives from the inherent crystal structure and their chemical potential in solution [35]. Most of rare earth hydroxides possess a hexagonal phase, similar to that of ZnO, which is well-known to exhibit anisotropic growth. This anisotropic structure suggests that $RE(OH)_3$ has a strong tendency toward 1D growth along the [0 0 1] direction, which leads to the formation of 1D nanostructures [25]. In detail, when the dissolved rare earth nitrates are gradually dropped into the alkaline solution (ammonia or NaOH) which provides the corresponding chemical potential at suitable temperatures, the original anions are substituted by stronger anions OH^- [40]. The nucleation of $RE(OH)_3$ would occur and there is an intrinsic tendency to crystallize into rod-like nanoparticles [41,42]. Overall, both the intrinsic structure and favorable extrinsic condition promote the formation of the nanorods. The possible formation mechanism of the $RE(OH)_3$ and REO_x nanorods is demonstrated in Scheme 1.

Fig. 7 shows the thermal properties of the $Eu(OH)_3$ sample synthesized using ammonia as the precipitation agent and after aging for 96 h. Three steps with a total weight loss of 18.4% were observed from 40 °C to 650 °C [29]. The first is desorption of water molecules from the surface of the sample, corresponding to 3.5% weight loss. However, the latter two steps can be ascribed to the decomposition of $Eu(OH)_3$ to EuOOH and of EuOOH to Eu_2O_3, respectively. The observed weight loss for the two processes is about 14.9%, in good agreement with a theoretical weight loss of 15.3% for the conversion of $Eu(OH)_3$ to Eu_2O_3 through EuOOH. Other $RE(OH)_3$ samples experience a similar thermal process (results not shown here). Based on the above TG analysis, the hydroxides can be converted into the corresponding oxides after thermal treatment at 650 °C for 2 h, as verified by the subsequent XRD results (Fig. 8). All diffraction peaks of these products belong to the cubic phase of RE_2O_3 (Pr_6O_{11}). The lattice constants (a) are listed in Table 1.

Fig. 9 shows the TEM (HRTEM) and/or FESEM images of the as-prepared REO_x samples. Although the nanorod (nanobundle) morphologies are preserved after calcination, a small shrinkage in sizes is distinguished, as shown in Table 1. This can be attributed to the dehydration of hydroxides resulting in a higher density. Specially, the Pr_6O_{11} sample consists of many nanoparticles due to the relatively small size of the $Pr(OH)_3$ nanorods. Similar to the hydroxides, the nanobundles for Sm, Eu and Gd oxides are clearly polycrystalline though the individual nanorod is a single crystal. As shown in the insets of Fig. 9d, the FFT pattern taken on the Eu_2O_3 nanobundle is consisted of several sets of FFT patterns, which could be obtained when the electron beam is focused on several individual nanorods with different axis zones. Because the Eu_2O_3 crystal is bundle-like morphology, it is difficult to focus the electron beam on a single nanorod. Based on the HRTEM images, all REO_x nanorods grow along [0 2 2] direction, which can be attributed to the variation from hexagonal structure for the hydroxides to cubic structure for the oxides.

The surface properties of the hydroxides and oxides were characterized by N_2 adsorption/desorption. As given in Table 1, the BET surface areas of $RE(OH)_3$ are much lower than those of REO_x.

Fig. 10 shows the room temperature PL spectra of the Eu_2O_3 nanobundles and bulk Eu_2O_3 (for reference). The TEM image (not shown here) shows that the bulk Eu_2O_3 obtained by thermal decomposition of europium nitrate at 650 °C for 2 h in air was aggregates of nanoparticles. As shown in Fig. 10b, the PL spectrum of bulk Eu_2O_3 is composed of the characteristic emission peaks of Eu^{3+}, corresponding to $^5D_0$–^7F_J (J = 0, 1, 2, 3) [43,44]. Among these emission peaks, the peak at 613 nm, which is a hypersensitive forced electric dipole transition ($^5D_0 \rightarrow {}^7F_2$) [45], is dominant in comparison with any other peaks. This indicates that the cubic phase has been produced [21,31]. As shown in Fig. 10a, only the $^5D_0 \rightarrow {}^7F_2$ transition peak is evident for the Eu_2O_3 nanobundles. Compared with bulk Eu_2O_3, the peak position for the Eu_2O_3 nanobundles has not shift, confirming the cubic structure. However, the peak intensity is obviously weakened concomitant with the peak broadening. This might be attributed to the lower scattering of evolved light and higher packing densities for nanoparticles than those for nanobundles [46]. Furthermore, the rough surfaces observed on nanobundles means the high concentration of inherent defects, which can lead to luminescence quenching [47]. Anyhow, the real reason needs further work.

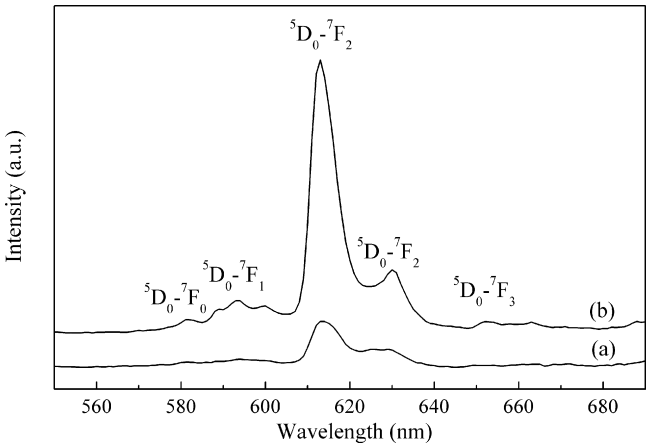

Fig. 10. Luminescent spectrum (excitation at 254 nm) of Eu_2O_3 at room temperature: (a) nanobundles and (b) bulk (obtained by thermal decomposition of europium nitrate at 650 °C for 2 h in air).

4. Conclusions

Rare earth hydroxide and oxide nanorods (nanobundles) with the diameter of 10–150 nm and the length of 30–600 nm have been synthesized without the addition of any templates/surfactants by a simple precipitation method under ambient temperature and pressure. The aspect ratio of the rods can be easily controlled by adjusting the aging time and the precipitation agents. The corresponding oxides can be obtained by calcination, which preserved the nanorod (nanobundle) morphologies though a small shrinkage in sizes is observed.

The crystallization mechanism is proposed. The nucleation and growth of the hydroxide nanorods may occur in the precipitation process at relatively low (room) temperature and normal pressure without a long-time and high-temperature (pressure) hydrothermal treatment.

Compared with the bulk Eu_2O_3, the $^5D_0 \rightarrow {}^7F_2$ transition peak of the Eu_2O_3 nanobundles is obviously weakened concomitant with the peak broadening.

The precipitation method is simple, highly reproducible, inexpensive, and widely applicable for the large-scale industrial production.

Acknowledgements

This work was supported by the 863 program of the Ministry of Science and Technology of the People's Republic of China (No. 2008AA06Z320), the National Natural Science Foundation of China (No. 20777028), the Natural Science Foundation of Shandong Province (No. Y2007B36) and the Program of the Development of Science and Technology of Shandong Province (No. 2008GG10003026).

References

[1] J. Shen, L.D. Sun, C.H. Yan, Dalton Trans. (2008) 5687.
[2] Z.G. Zhou, H. Hu, H. Yang, T. Yi, K.W. Huang, M.X. Yu, F.Y. Li, C.H. Huang, Chem. Commun. (2008) 4786.
[3] Z.H. Xu, C.X. Li, P.P. Yang, C.M. Zhang, S.S. Huang, J. Lin, Cryst. Growth Des. 9 (2009) 4752.
[4] P. Mele, C. Artini, A. Ubaldini, G.A. Costa, M.M. Carnasciali, R. Masini, J. Phys. Chem. Solids 70 (2009) 276.
[5] J.H. Zhou, J.P. He, T. Wang, X. Chen, D. Sun, Electrochim. Acta 54 (2009) 3103.
[6] H. Inoue, S. Sato, R. Takahashi, Y. Izawa, H. Ohno, K. Takahashi, Appl. Catal. A 352 (2009) 66.
[7] A.W. Xu, Y. Gao, H.Q. Liu, J. Catal. 207 (2002) 151.
[8] G.Y. Adachi, N. Imanaka, Chem. Rev. 98 (1998) 1479.
[9] H. Maas, A. Currao, G. Calzaferri, Angew. Chem. Int. Ed. 41 (2002) 2495.
[10] X. Wang, Y.D. Li, Chem. Eur. J. 9 (2003) 5627.
[11] Y.N. Xia, P.D. Yang, Y.G. Sun, Y.Y. Wu, B. Mayers, B. Gates, Y.D. Yin, F. Kim, H.Q. Yan, Adv. Mater. 15 (2003) 353.
[12] S.V.N.T. Kuchibhatla, A.S. Karakoti, D. Bera, S. Seal, Prog. Mater. Sci. 52 (2007) 699.
[13] J.T. Hu, T.W. Odom, C.M. Lieber, Acc. Chem. Res. 32 (1999) 435.
[14] X. Wang, Y.D. Li, Inorg. Chem. 45 (2006) 7522.
[15] A.W. Xu, Y.P. Fang, L.P. You, H.Q. Liu, J. Am. Chem. Soc. 125 (2003) 1494.
[16] G.R. Patzke, F. Krumeich, R. Nesper, Angew. Chem. Int. Ed. 41 (2002) 2446.
[17] C.G. Hu, H. Liu, W.T. Dong, Y.Y. Zhang, G. Bao, C.S. Lao, Z.L. Wang, Adv. Mater. 19 (2007) 470.
[18] X.W. Xie, Y. Li, Z.Q. Liu, M. Haruta, W.J. Shen, Nature 458 (2009) 746.
[19] F. Chen, R.J. Zhou, L.G. Yang, M.M. Shi, G. Wu, M. Wang, H.Z. Chen, J. Phys. Chem. C 112 (2008) 13457.
[20] Y.F. Hsu, Y.Y. Xi, K.H. Tam, A.B. Djurišić, J.M. Luo, C.C. Ling, C.K. Cheung, A.M.C. Ng, W.K. Chan, X. Deng, C.D. Beling, S. Fung, K.W. Cheah, P.W.K. Fong, C.C. Surya, Adv. Funct. Mater. 18 (2008) 1020.
[21] T.T. Yan, D.S. Zhang, L.Y. Shi, H.R. Li, J. Alloys Compd. 487 (2009) 483.
[22] L.X. Zhang, H.F. Jiu, J. Luo, Q.W. Chen, J. Cryst. Growth 309 (2007) 192.
[23] L. Shi, G.L. Dong, D.H. He, Catal. Commun. 8 (2007) 359.
[24] P.X. Huang, F. Wu, B.L. Zhu, G.R. Li, Y.L. Wang, X.P. Gao, H.Y. Zhu, T.Y. Yan, W.P. Huang, S.M. Zhang, D.Y. Song, J. Phys. Chem. B 110 (2006) 1614.
[25] X. Wang, Y.D. Li, Angew. Chem. Int. Ed. 41 (2002) 4790.
[26] N. Zhang, R. Yi, L.B. Zhou, G.H. Gao, R.R. Shi, G.Z. Qiu, X.H. Liu, Mater. Chem. Phys. 114 (2009) 160.
[27] L. Ma, W.X. Chen, J. Zhao, Y.F. Zheng, J. Cryst. Growth 303 (2007) 590.
[28] M. Mazloumi, N. Shahcheraghi, A. Kajbafvala, S. Zanganeh, A. Lak, M.S. Mohajerani, S.K. Sadrnezhaad, J. Alloys Compd. 473 (2009) 283.
[29] V.G. Pol, O. Palchik, A. Gedanken, I. Felner, J. Phys. Chem. B 106 (2002) 9737.
[30] L. Yan, R.B. Yu, G.R. Liu, X.R. Xing, Scripta Mater. 58 (2008) 707.
[31] G.S. Wu, L.D. Zhang, B.C. Cheng, T. Xie, X.Y. Yuan, J. Am. Chem. Soc. 126 (2004) 5976.
[32] L.W. Qian, Y.C. Gui, S. Guo, Q. Gong, X.F. Qian, J. Phys. Chem. Solids 70 (2009) 688.
[33] B.L. Cushing, V.L. Kolesnichenko, C.J. O'Connor, Chem. Rev. 104 (2004) 3893.
[34] S. Sato, R. Takahashi, M. Kobune, H. Gotoh, Appl. Catal. A 356 (2009) 57.
[35] B. Hou, Y. Xu, D. Wu, Y.H. Sun, J. Mater. Sci. 42 (2007) 1397.
[36] A.S. Karakoti, S.V.N.T. Kuchibhatla, D.R. Baer, S. Thevuthasan, D.C. Sayle, S. Seal, Small 4 (2008) 1210.
[37] X.C. Wu, Y.R. Tao, F. Gao, L. Dong, Z. Hu, J. Cryst. Growth 277 (2005) 643.
[38] M.J. Siegfried, K.S. Choi, Adv. Mater. 16 (2004) 1743.
[39] M.J. Siegfried, K.S. Choi, Angew. Chem. Int. Ed. 44 (2005) 3218.
[40] S.C. Kuiry, E. Megen, S.D. Patil, S.A. Deshpande, S. Seal, J. Phys. Chem. B 109 (2005) 3868.
[41] S.C. Kuiry, S.D. Patil, S. Deshpande, S. Seal, J. Phys. Chem. B 109 (2005) 6936.
[42] Q. Tang, Z.P. Liu, S. Li, S.Y. Zhang, X.M. Liu, Y.T. Qian, J. Cryst. Growth 259 (2003) 208.
[43] Kumar, S. Babu, A.S. Karakoti, A. Schulte, S. Seal, Langmuir 25 (2009) 10998.
[44] S. Babu, A. Schulte, S. Seal, Appl. Phys. Lett. 92 (2008) 123112.
[45] W.Q. Fan, S.Y. Song, J. Feng, Y.Q. Lei, G.L. Zheng, H.J. Zhang, J. Phys. Chem. C 112 (2008) 19939.
[46] L.S. Wang, Y.H. Zhou, Z.W. Quan, J. Lin, Mater. Lett. 59 (2005) 1130.
[47] W. Li, J. Lee, J. Phys. Chem. C 112 (2008) 11679.